Indian Journal of Chemistry
Vol. 62, October 2023, pp. 1012-1029
DOI: 10.56042/ijc.v62i10.3779

3D-QSAR, molecular docking and ADME studies on indole analogues reveal antidepressant activity through monoamine oxidase-A inhibition

Alka Kumari[a], Harnoor Kaur[a], Priyanka Rana[a], Tanzeer Kaur[b], Poonam Arora[c] & Neelima Dhingra*[a]

[a] University Institute of Pharmaceutical Sciences, Panjab University Chandigarh 160 014, India

[b] Department of Biophysics, Panjab University Chandigarh 160 014, India

[c] Chitkara College of Pharmacy, Chitkara University, Rajpura, Patiala 140 401, India

E-mail: neelimad08@gmail.com

Received 19 July 2023; accepted(revised) 22 September 2023

Monoamine oxidase (MAO) enzymes over see the concentration of neurotransmitters and intracellular amines in the brain and peripheral tissues by catalysing their oxidative deamination and represents a crucial target in drug designing for the management of neurological and psychiatric disorders. Present study is an effort to present an economical fast high throughput screening easy method to identify indole analogues as potent MAO inhibitors, using different computational techniques. CoMSIA field-based 3D-QSAR models have been developed by applying the partial least squares regression algorithm that exhibit satisfactory predictive and descriptive capability with statistical parameters R^2 (0.9557) and Q^2 (0.8529). Generated model (s) helped in explaining the key descriptors firmly related with MAO inhibitory activity and are used to generate library of 1853 indole derivatives. Library is evaluated and has resulted in the identification of 30 indole derivatives with high docking scores (−9.978 to −7.136) in comparison to the antidepressant standard drug Isocarboxazid (−7.125). Further, these compounds have been scrutinized through drug-likeliness profiles and Desmond's molecular dynamics simulations studies for 100 ns. Further *in vitro* and *in vivo* studies on these molecules might provide us with new drug candidate for the treatment of depression with high therapeutic index.

Keywords: Depression, MAO-A, Indole derivatives, QSAR, Docking, ADME

In the past twenty years, the view of the path involved and essence of the most commonly diagnosed mental disorder depression has altered dramatically[1]. Signs and severity of symptoms ranging from a prolonged feeling of sadness, loss of interest in joyful activities, insomnia or oversleeping, weight loss or weight gain, feeling of worthless, suicidal thoughts, *etc*. vary from person to person and age group[2]. Monoamine oxidase inhibitors (MAOIs) were the first to be authorised for the treatment of depression[3], and represented classical therapeutic use in the major depressive disorder, bipolar depression, including resistant depression. A maximum of the antidepressants available in recent times are known to act by enhancing the activity of monoamine neurotransmitters either by inhibiting the activity of an enzyme or by reuptake inhibition[4]. Monoamine oxidases (MAOs) are iron containing flavoenzymes that catalyse the oxidative deamination of amines, neurotransmitters, and thus control their concentrations in brain and peripheral tissues[5]. Two isoforms of MAOs i.e. MAO-A and MAO-B have been identified and characterized. Serotonin, norepinephrine, and epinephrine monoamines are oxidized by MAO-A and whereas phenylethylamine and benzylamine are suitable substrate for MAO-B[6]. The indole scaffold represents some of the most relevant structural subunit in the drug discovery process of new drug candidates including design of MAO inhibitors in the treatment of depression (Fig. 1).

The prospect of using the indole moiety in the creation of MAO inhibitors continued and resulted in the synthesis of variety of indole derivatives, followed by their *in vitro* and *in vivo* testing using human MAO-A enzyme[7]. Indole moiety has been found to be highly reactive towards electrophilic substitution reactions especially at position-3, the most preferred

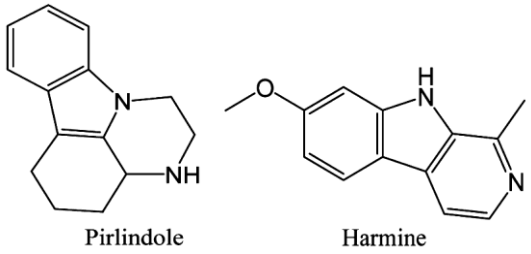

Pirlindole Harmine

Fig. 1 — Antidepressant drugs containing Indole moiety

place for substitution[8]. Therefore, considering the prospect of using the Indole moiety in the development of MAO inhibitors, and importance of 3rd position in connecting additional heterocyclic rings, it was envisaged to exploit indole moiety for further possible modifications at 3rd position, with respect to the information available in the literature.

In silico methods including CoMSIA (Comparative Molecular Similarity Indices Analysis) based quantitative structure–activity relationship studies (QSARs), receptor ligand interaction (docking) and pharmacodynamics (absorption–distribution–metabolism–excretion) properties are the key steps presently being employed in drug discovery and development processes[9]. These methodologies have resulted into goal oriented drug discovery process with less consumption of resources like time and money and offered the advantage with their ability to predict the large number of molecules rapidly in a high-throughput mode[10]. Present work aimed to design and identify potent Indole-3-yl-amide **(1)** derivatives as MAOIs, based on the information from statistically significant QSAR models, molecular docking, dynamic and ADME prediction regarding important physio chemical parameters to get more potent and selective MAO inhibitors.

Experimental Section

Quantitative Structure Activity Relationship (QSAR)

In the current study, CoMSIA field based QSAR models were generated considering electrostatic, hydrophobic, or steric fields, for a set of aligned ligands. Maestro 12.3 version of the Schrodinger suite (Schrodinger, LLC, NY USA) including LigPrep, Glide docking, Grid generation, QikProp *etc*. was used to carry out the entire computational analyses.

Dataset collection

The selected data set to construct the models defines the quality of the QSAR model. A total number of 28 indole derivatives were collected from the literature with different pharmacological activities, wherein their i*n vitro* biological activity stated their ability inhibit MAO by 50% (IC_{50}). And to generate PLS regressed 3D-QSAR (CoMSIA) models, the IC_{50} values were transformed into negative logarithmic forms pIC_{50} (pIC_{50} = 9 - log 10(IC_{50})) and was used as dependent variable along with descriptor of field intensities as an independent variable[11]. ChemDraw drawing tool was used to establish the 2D structure of the compounds.

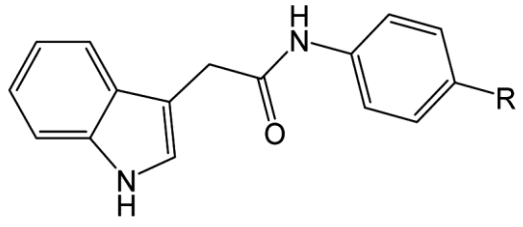

(1) Indole-3-yl-amide

Selection of training and test set

The experimental dataset included a wide spectrum of compounds, ranging from moderately active to very active. And the dataset of 28 molecules was randomly divided into training & test with 70% and 30% molecules, and maximum partial least squares (PLS) factor of 4 (12) for generation of field-based model. Twenty molecules were chosen at random for the training set and 8 molecules picked at random for the test set. To get a deep insight into structure and activity correlations, training set was used to construct CoMSIAmodels based on steric and electrostatic fields, whereas the test set was used for the model validation.

Ligand preparation and ligand alignment

Maestro Schrodinger 12.3 was used to transform the 2D geometry of selected 28 indole derivatives into 3D structures. LigPrep module was used to generate energy-minimized 3D conformations of inhibitors, followed by hydrogen addition, tautomers production, and generation of one conformation with lowest energy. Ionization state at *p*H 7.0 ± 2.0 were generated using Epik module and optimized potential for liquid simulations 2005 (OPLS_2005) adopted to achieve energy minimization. Most important input for creating CoMSIA field-based 3D-QSAR models is molecular alignment. Flexible Ligand Alignment panel (Tools menu) in the Schrodinger software was used to align the ligands. The goal of the alignment is to obtain optimal alignment between the molecular structures necessary for ligand-receptor interactions.

Regression analysis

QSAR, a parametric approach was applied on the selected set of compounds to understand crucial structural factors responsible for their activity. Partial Least Square method coupled with Monte-Carlo algorithm was involved in the building of QSAR

model. Statistical parameters that are used to evaluate the generated models are the standard deviation (SD), correlation coefficient of training set (R^2), cross-validated correlation coefficient (R^2CV), F value, stability, root mean square error (RMSE), correlation coefficient for test set (q^2), and Pearson-r. The F-value reflects the ratio of the variance and its high values in developed models indicate the statistical significance of models. Further, high value of stability and lowest of Pearson-r and RMSE indicates the fitness of model[13].

CoMSIA field-based 3D-QSAR model generation and validation

CoMSIA method centered on the assumption of correlation between changes in a molecule's binding affinity and properties stated as molecular fields. PHASE module incorporated in Schrödinger's Maestro interface was used to create CoMSIA QSAR models from a set of generated ligands, using partial least square (PLS) technique. PHASE module gives the basis of building the CoMSIA models using the ligands activities that matches a reported hypothesis.

Stability and predictive power of generated models were assessed using leave-one-out (LOO) cross-validation method. The best model was selected on the basis of statistical parameters like root mean square error of the test set (RMSE), (R^2), the coefficient of determination for test set, significance level of variance ratio (F factor), Q^2 value (the predicted activities of the test set, Pearson-r (the predictive ability of the model) including standard deviation (SD) as some of the crucial parameters. The number of PLS factors were also restricted to avoid over-fit models. Scatter plots were presented by correlating the observed and predicted activity of the data set molecules. The QSAR visualization for CoMSIA field-based models was performed in the form of the 3D contour maps associated with structural features.

Molecular Docking

Maestro 12.3 version of the Schrodinger suite (Schrodinger, LLC, NY USA) including LigPrep, Glide docking, Grid generation, QikProp *etc*. was used to carry out the entire computational analyses.

Library enumeration and ligand preparation

Present study aimed in identifying novel compounds with a potential to have good MAO inhibitory activity, and Indole skeleton was used to achieve the aforementioned aim. It's a medicinally relevant scaffold and has become a privileged structure or pharmacophore due to its different pharmacological actions[16]. Proposed Indole skeleton (Indole-3-yl-amide) was drawn and varied derivatives designed by incorporating (un)/substituted side-chains at 3rd position of the chosen skeleton to get a library of total 1853 derivatives using 3D Builder Panel of the Schrodinger suite (Maestro 12.3). The ligands were prepared in sequential manner, following the protocol described in LigPrep module of Maestro 12 followed by energy minimization for each ligand till it reached a root mean square deviation (RMSD) cut off of 1.8 Å. Ligand, with best conformer with minimum potential energy was selected for molecular dynamic simulation studies.

Protein preparation and grid generation

Crystallographic structure of MAO-A enzyme (PDB ID: 2Z5X) in complex with Harmine at resolution 2.20 Å was downloaded from Protein Data Bank (www.rcsb.org). Optimization of receptor was done using protein preparation wizard of Maestro 12.3, and pre-processed and refined for formal charges, bond orders and addition of missing hydrogen atoms along with other residues or co-factors. As water molecules are usually not involved in the binding, so all water molecules (except those coordinated to metals) are deleted, but occasionally waters that bridge between the ligand and the protein are retained. Following Schrodinger suite protocol, water molecules beyond 5 Å were eliminated and possible ionization states in the protein structure were produced to select the most stable form[17]. Removal of these water molecules with possibility to distort the poses from binding pocket enable the computation process smoother and easy. But in conditions with retention of water molecules, hydrogens were added and their orientation corrected during the preparation component of the protein preparation job. The hydrogen bonds were assigned, and energy minimization of the prepared protein structure was carried out using OPLS2005 force field to reorient side-chain hydroxyl groups. The steric unfavourable and repulsive interactions were minimized and successfully employed for docking of generated MAOIs .

A grid represents the shape and properties of active sites of protein and is searched prior to docking studies. Druggable site of the prepared protein is being defined by set of amino acid residues available in the active site

and involved with cocrystallized ligand in protein[18]. In the present study, a grid was created employing Receptor Grid Generation panel of GLIDE tool in the Schrodinger suite (Maestro 12.3 version), and receptor grid was constructed by retaining the ligand HRM in the crystal structure of the prepared protein. The binding box dimensions (within which the centroid of a docked pose is confined) of the protein was set to 14 Å x 14 Å x 14 Å.

Ligand docking

Molecular docking of the prepared ligands was performed employing extra precision ligand docking panel of GLIDE tool in the Maestro interface. Favourable conformations of ligand in the active site of protein were searched using a series of hierarchical filters and docked studies were executed using generated grid. Extra precision mode of ligand docking panel was chosen to weed out the false positives and to get a better correlation between the poses and the scores[19]. The ligand forming a most stable drug-receptor complex is the one with minimum dock (D) score and the best docked conformer of all the ligands was checked for various interactions like hydrogen, hydrophobic, aromatic and Vander Waals interactions.

In silico ADME Prediction

A drug candidate's performance is measured not only by its high therapeutic potential, but also by a favourable ADME profile. Almost 40% of drug candidates fail in clinical trials on account of weak ADME properties. The QikProp module in Schrodinger software 12.3 was used to investigate the ADME properties of ligands in generated library. The server calculated the parameters such as human oral absorptivity (HOA%), Caco-2 *in vitro* and Maden Darby Canine Kidney (MDCK) cellular permeability, plasma protein binding (PPB) and (QPlogBB) permeability.

Molecular Simulation Studies

The docked complexes of the proteins were used for performing the MD simulations. The Desmond software of the Schrodinger Suite was used to perform the MD simulation for the top four docked complexes. The complexes were placed in an orthorhombic box with the dimensions of 10.0 Å × 10.0 Å × 10.0 Å, which was then solvated with the TIP3P water model and 0.15 M NaCl ions. The OPLS4 force field with default values was used to conduct molecular minimization and molecular dynamics simulation. The 5 complexes were used for 100 ns MD simulations in the NPT ensemble after equilibration. Stability of the bounded complex (protein and ligand) after completion of the simulation was analyzed by root mean square deviation (RMSD), root mean square fluctuation (RMSF), protein-ligand contacts, and interaction percentages maintained during the MD simulation.

Results and Discussion

Quantitative Structure Activity Relationship (QSAR)

Quantitative structure-activity relationship modelling is one of the latest computational tools being employed in medicinal chemistry. It relies on the basic principle of chemistry, and relates the therapeutic activity of the ligand/compound with the arrangement of atoms forming its molecular structure, where in this structural data is defined as molecular descriptors. The CoMSIA field-based QSAR models were created using partial least square (PLS), correlating five fields: steric, electrostatic, hydrophobic, hydrogen bond donor (HBD), and hydrogen bond acceptor (HBA)[20]. The Maestro 12.3 version of the Schrodinger suite (Schrodinger, LLC New York, NY USA) including PHASE, Flexible Ligand Alignment, CoMSIA field based QSAR was used to carry out the entire computational analyses. The set of training and test molecules are shown in Table 1 and Table 2.

For a given set of aligned ligands, 3D QSAR models were build based on electrostatic, hydrophobic, or steric fields. The developed CoMSIA field -based 3D QSAR models correlated the steric and electrostatic field intensities of the training set, using PLS-4 with five components. Around two hundred models (190) were developed using a training set of 28 molecules (Table 1 and Table 2) and Table 3 holds the statistically significant top four models with good predictive power.

Internal validation method was used to improve the reliability of the created 3D-QSAR models. The leave-one-out (LOO) cross-validation approach was used to assess the robustness, stability, and predictive capability of models. The internal validation by the LOO further revealed the best model (Table 4) for training set with (Q^2 = 0.8529, coefficient of determination for the test set (R^2= 0.9557), standard deviation (SD = 0.1765), root mean square error (RMSE = 0.65), significance level of variance ratio

Table 1 — Data set for QSAR models

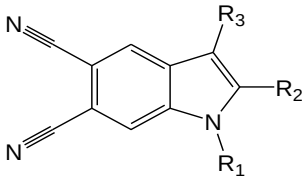

Indole-5,6-dicarbonitrile derivatives

Series 1

Sr. No	R_1	R_2	R_3	QSAR set	Actual IC50	Predicted pIC50
A1	OH	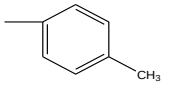	H	Training	1.14	5.943
A2	OH	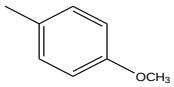	H	Training	1.84	5.735
A3	OCH_3	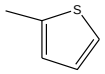	H	Training	11.1	4.995
A4	OCH_3	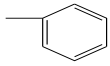	CHO	Test	0.522	6.282
A5	OCH_3	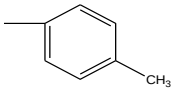	CHO	Training	0.405	6.939
A6	OCH_3	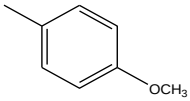	CHO	Training	0.147	6.833
A7	OCH_3	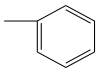	CH_2OH	Test	4.99	5.302
A8	OCH_3	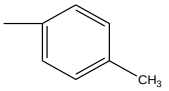	CH_2OH	Training	5.12	5.291
A9	OCH_3	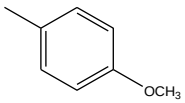	CH_2OH	Test	1.13	5.947

(P = 0.755e-10). Testing set with eight molecules was used to validate the model by predicting their pIC_{50} values and the predictive correlation coefficient (Q^2 value) indicated the reasonable predictive potential of models.

CoMSIA method calculated five conventional Gaussian fields i.e. Gaussian steric, hydrophobic, electrostatic, H-bond acceptor and donor field. Gaussian aromatic ring field, illustrated that the substituents on N-1, C-2, C-3, C-5 and C-6 of the indole ring may add differently towards the activity. A contour map for steric factor (Fig. 2a) with green and red regions on the molecules represents the favorable or unfavorable effects of bulky substituents at the respective places. Increase in the activity was observed with OCH_3 and methylbenzene ring at the 1st and 2nd position of the indole ring in derivative 5, 8 respectively, whereas compound 4 indicated fall in the activity with CHO group at 3rd position. Fig. 2b represents the contour map for electrostatic factor and respective blue and red regions on the molecules indicate the favorable or unfavorable effects of electropositive substituents at the respective places. Red color around the 2nd, 3rd, 5thand 6th position of indole ring in compounds 21 and 27, with unfavorable indications for electropositive group, showing increased activity on account of presence of electronegative groups. Further, presence of electropositive moiety added towards the MAO inhibitory activity of derivative 5 and 6 with OCH_3 group at

Table 2 — Data set for QSAR models

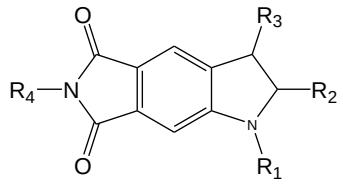

Pyrrolo-3,4-indol-5,7-dione derivatives

Series 2

Sr. no	R_1	R_2	R_3	R_4	QSAR set	Actual IC50	Predicted pIC50
A10	OH	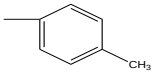	H	H	Test	1.16	5.936
A11	OH	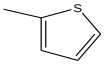	H	H	Training	6.35	5.197
A12	OCH_3	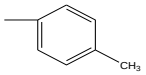	H	H	Training	1.75	5.757
A13	OCH_3		H	H	Training	6.70	5.174
A14	OCH_3		H	CH_3	Training	1.24	5.907
A15	H		Cl	H	Training	0.250	6.602
A16	$COOCH_3$	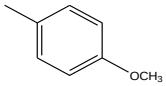	CH_3	H	Training	3.57	5.447
A17	$COOC_2H_5$	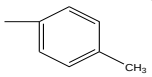	C_2H_5	CH_3	Training	22.2	4.654
A18	$COOnC_3H_7$	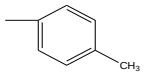	nC_3H_7	H	Training	22	4.658
A19	OH		CH_3	H	Training	21.4	4.666
A20	OH	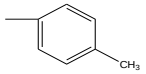	C_2H_5	CH_3	Test	17.9	4.747
A21	OH		C_2H_5	Cl	Training	16.6	4.78
A22	H	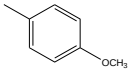	-	Cl	Test	0.813	6.09
A23	OH		-	H	Training	45.6	4.341
A24	OH	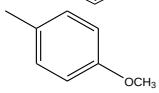	-	H	Training	21.6	4.666
A25	H		Cl	Cl	Test	31.4	4.508
A26	OH		-	Cl	Training	7.67	5.115
A27	Cl	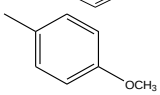	Cl	-	Training	9.79	5.009
A28	OH	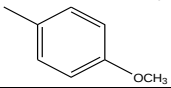	Cl	Cl	Test	69.42	4.159

Table 3 — Parameters of the CoMSIAfield-based QSAR model

Factors	SD	R^2	R^2 CV	R^2 scramble	Stability	F	P	RMSE	Q^2	Pearson-r
1	0.6169	0.3503	0.002	0.2885	0.865	9.7	0.005	0.58	0.2270	0.5150
2	0.4709	0.6425	0.072	0.5009	0.586	15.3	0.001	0.50	0.4200	0.6731
3	0.2583	0.8988	0.0322	0.6554	0.255	47.4	3.51e-08	0.27	0.8366	0.9157
4	0.1765	0.9557	0.2228	0.7443	0.324	80.9	0.75e-10	0.25	0.8529	0.9460

Table 4 — of the best CoMSIAfield-based QSAR model

Factors	SD	R^2	R^2CV	R^2 scramble	Stability	F	P	RMSE	Q^2	Pearson-r
4	0.1765	0.9557	0.2228	0.7443	0.324	80.9	0.75e-10	0.25	0.8529	0.9460

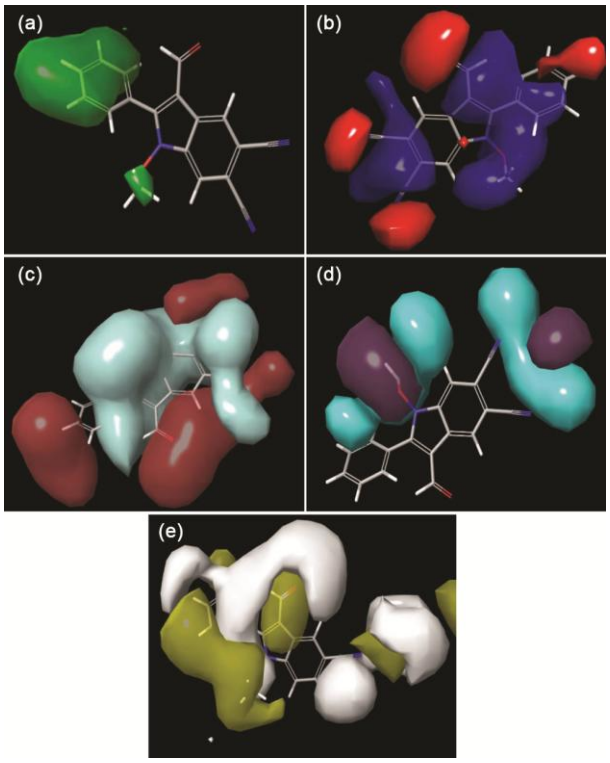

Fig. 2 — 2a Steric counter map; favourable (green), unfavourable (red) 2b Electrostatic counter map; electropositive favourable (blue), electronegative favourable (red) 2c Hydrophobic counter map; favourable (yellow), unfavourable (grey) 2d HBA counter map; favourable (red), unfavourable (white) 2e HBD counter map favourable (violet), unfavourable (cyan).

the 1st position of indole ring. Contour maps for hydrophobic factor (Fig. 2c) with yellow and grey regions on the molecules represent the favorable or unfavorable effects of hydrophobic substituents at the respective places. Increase in the activity was observed with phenyl ring and CHO group at the 2nd and 3rd position of the indole ring in derivative 23, 6 respectively, whereas compound 12 indicated fall in the activity with OCH_3 group at the 1st position.

Contour map for Hydrogen bond acceptor (HBA) factor and interactions are being represented in

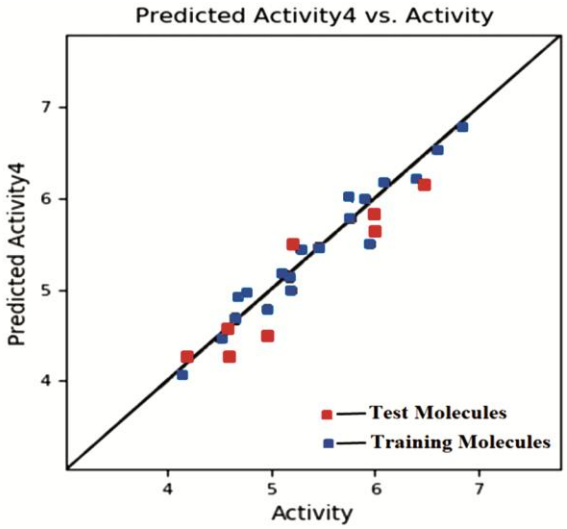

Fig. 3 — Graphical presentation of actual *versus* predicted pIC50 in test (red) and training (blue) molecules.

Fig. 2d along with favourable or unfavourable effects of HBA substituents in red and white regions on the molecules. Substitution with HBA moieties like Cl and methoxybenzene at the 1st and 2nd position of indole ring added toward the MAO-A inhibitory activity of molecules **27** and **9** respectively, whereas decreased activity with HBA moieties was observed in derivative **6** with CHO group at the 3rd position. Contour maps for hydrogen bond donor (HBD) factor (Fig. 2e) with violet and cyan regions on the molecules are representing the favorable or unfavorable effects of hydrogen bond donor (HBD) moieties. Groups that are closer to the cyan contour are inactive in the molecules. Increase in the activity was observed with OH and CH_2OH groups at the 1st and 3rd position of the indole ring in derivative **11, 8** respectively, whereas compound **4** indicated fall in the activity with phenyl ring at 2nd position.

The plots of the actual vs. predicted binding affinities for both the test and training set MAO inhibitors shown in Fig. 3 are representing the

Gaussian-based 3D-QSAR models. And assessment of experimentally observed and predicted IC_{50} values, indicated the better performance of 3D QSAR Gaussian model in prediction of the activities for both test and training molecules.

Among the privileged indole nucleus with different substituents at various positions, so far 2- and 3-functionalized indoles represents the most promising candidates with antidepressant activities. And in the present paper, CoMSIA based 3D-QSAR models were built and rigorously validated using series 1 (indole-5,6-dicarbonitrile derivatives) and series 2 (pyrrolo 3,4 indole-5,7-dione derivatives). QSAR counter maps from the generated models gave information about the set of field points, and revealed the key regulatory features associated with the antidepressant activity of the compounds. With the advances in computer science and interest to find novel indole derivative with possible modification and can bind the desired receptors, a library (1853) was generated using available tool library enumeration in Schrodinger suite, (s). Virtual screening approach like docking and ADME filters and molecular simulation studies were conceded in filtering many compounds.

Molecular Docking

Molecular docking, a structure-based scoring strategy is used to predict the interaction between ligands and their potential molecular targets. It is gaining a status of important drug discovery tool and workflow starts by predicting the possible molecular orientations of a ligand within a receptor and then scoring such orientations to estimate the best complementarity possible conformation[21]. This scoring function compares the type range of interactions, and their binding energies, that select and enable best ligand-target pairs to move further in the drug development process[22].

Docking simulations (*in silico*) studies were performed on the generated library of 1853 compounds using Glide Docking module available in The Maestro 12.3 version of the Schrodinger suite with active site (**2Z5X**) of MAO-A receptors. Isocarboxazid known to possess affinity for MAO receptors (**2Z5X**), was also included in the docking studies for comparison. The extent of binding between ligand and protein i.e. binding affinity represented by scoring function known as D-score is shown in Table 5 for 30 compounds.

Minimum is the D score, greater is affinity of a particular ligand for a given receptor. Isocarboxazid (standard drug) having D-score (−7.126) showed crucial hydrophobic interactions with amino acid residues TYR69, MET350, PHE352, ILE180, PHE208, LEU97, ILE325, CYS323, ILE335, LEU337, TYR444, ILE207, TYR197, TYR407, VAL210, along with pi-pi stacking interaction with amino acid PHE208, and aromatic bonding with HOH 726 residues as indicated in Fig. 4a,b. For the generated library of indole, docking score was observed in the range from 9.978 to −2.770 and top 30 compounds (**IND-1to IND-30)** (Table 5) were identified for further studies. Docking behavior of these 30 molecules was observed in comparison to the Isocarboxazid (reference) drug, by interacting with common active residues LEU97, LEU337, ILE180, ILE207, ILE325, TYR197, TYR444, TYR69, MET350, PHE352, PHE208 and strong hydrophobic bonds. Further, additional hydrophobic bonding, pi-pi stacking interactions and aromatic interactions could be contributing factor for the high score of (IND-1 to IND- 30). The docked poses of the fitted ligands visualized by extending deep into the active site pocket showed the presence of Vander Waals, hydrophobic, aromatic and π-π stacking interactions with the key residues of the active site. Fig. 5a,b - 9a,bare the 2D and 3D representations of the ligand interactions of standard drug and compounds that have an excellent docking score, with the receptor of MAO receptors (2Z5X), respectively.

Complimentary shape and greater number of amino acid residues, more hydrophobic interactions, and more aromatic interactions have added to highest affinity of IND 1 (−9.978) for MAO-A receptor. Fig. 5a,b showing the aromatic bonding with active residue PHE208, and more p-pi stacking with residues TYR69, PHE35 of IND 1. Additional pi-pi stacking with residues PHE352, TYR69 in IND-2 to IND-4 (Fig. 6a,b, Fig. 7a,b, Fig. 8a,b and Fig. 9a,b) might be adding to their high score and less energy in comparison to reference drug.

In silico ADME Prediction

A critical piece in drug discovery and development is conducting DMPK (Drug Metabolism and Pharmacokinetics) studies, often referred to as ADMET (Absorption, Distribution, Metabolism, Elimination, Toxicity) studies. These studies help to determine the viability of a drug candidate. Number

Table 5 — D-score of 30 ligands and type of interactions involved in MAO-receptor

S.No	Compd	D-Score	No. Of Residues	Hydrophobic	Aromatic	Pi-Pi Stacking
1	Isocarboxaid	−7.126	18	TYR69,MET350,PHE352, ILE180, PHE208, LEU97, ILE325, CYS323,ILE335, LEU337,TYR444,ILE207, TYR197,TYR407,VAL210	HOH726	PHE208
2	**IND-1**	−9.978	23	ALA68, TYR69, MET350, PHE352, ILE180,PHE208, LEU97, ILE325, CYS323, ILE335, LEU337,TYR444, MET445,CYS406,TYR407, VAL303	HOH726, PHE208	HOH726, PHE208
3	**IND-2**	−9.755	26	ALA68, TYR69, MET350, PHE352, ILE180, ALA111, MET445,TRP397, PHE208, LEU97, ILE325, CYS323, ILE335, LEU337, TYR444, MET445,CYS406,TYR407, VAL303, VAL210	HOH726,	PHE352, PHE208, TYR69
4	**IND-3**	−9.418	25	ALA68, TYR69, MET350, PHE352, ILE180, VAL210, PHE208, ALA111, LEU97, ILE325, CYS323, ILE335, LEU337,TYR407,CYS406, TYR444,MET445,VAL303	-	PHE352, PHE208, TYR69
5	**IND-4**	−9.226	23	TYR69, ALA68, MET445, TYR444, ILE180, ILE325, CYS323, LEU97, VAL210, PHE208, ILE335, LEU337, PHE352,MET350,TYR407, CYS406, VAL303	-	PHE352, PHE208, TYR69
6	**IND-5**	−9.134	26	ALA68, TYR69, ILE180, PHE352,MET350,LEU337, ILE335, PHE208, VAL210, LEU97, CYS323, ILE325, PHE108,ALA111,TYR444, MET445,CYS406,TYR407, TRP397	HOH726 ARG51	PHE352, TYR69
7	**IND-6**	−9.037	25	ALA68, TYR69, VAL303, TYR407,CYS406,TYR444, MET445, LEU337, ILE335, ILE180, ILE325, CYS323, PHE208, VAL201, LEU97, ALA111,MET350, PHE352	-	PHE352, PHE208, TYR69
8	**IND-7**	−8.997	23	ALA68, TYR69, MET350, PHE352, LEU337, ILE335, ILE180, ILE325, CYS323, PHE208, VAL201, LEU97, TYR444, MET445, CYS406, TYR407, TRP397	HOH726	PHE208, TYR69
9	**IND-8**	−8.967	23	ALA68, TYR69, MET350, PHE352, LEU337, ILE335, ILE180, ILE325, CYS323, PHE208, VAL201, LEU97, TYR444, VAL65, CYS406, TYR407, TRP397	-	PHE208, TYR69
10	**IND-9**	−8.891	26	ALA68, TYR69, MET350, PHE352, LEU337, ILE335, ILE180, ILE325, CYS323, PHE208, VAL201, LEU97, PHE108,ALA111,TYR444, MET445,CYS406,TYR407, VAL303	-	PHE352, PHE208, TYR69
11	**IND-10**	−8.846	26	ALA68, TYR69, MET350, PHE352, LEU337, ILE335, CYS323, LEU97, PHE108, ALA111,PHE208,VAL210, ILE180, TYR444, MET445, VAL303,TYR407,CYS406, ILE325	HOH726, PHE352	PHE352, TYR69
12	**IND-11**	−8.825	26	ALA68, TYR69, MET350, PHE352,VAL210, PHE208, ILE335, LEU337, CYS323, ILE325, LEU97, PHE108, ALA111, ILE180, TYR444, MET445,CYS406,TYR407, VAL303	-	PHE352, PHE208, TYR69
13	**IND-12**	−8.768	25	ALA68, TYR69, MET350, PHE352,VAL210, PHE208, ILE335, LEU337, CYS323, ILE325, LEU97, ALA111, ILE180, TYR444, MET445, CYS406,TYR407, VAL303	PHE351	-

(contd.)

Table 5 — D-score of 30 ligands and type of interactions involved in MAO-receptor (*contd*.)

S.No	Compd	D-Score	No. Of Residues	Hydrophobic	Aromatic	Pi-Pi Stacking
14	**IND-13**	−8.709	25	ALA68, TYR69, MET350, PHE352, PHE208, ILE335, LEU337, CYS323, ILE325, LEU97, ILE180, TYR444, MET445,CYS406,TYR407, TRP397, VAL210	HOH726	PHE352, PHE208, TYR69
15	**IND-14**	−8.681	24	ALA68, TYR69, MET350, PHE352, PHE208, ILE335, LEU337, CYS323, ILE325, LEU97, ILE180, TYR444, MET445, CYS406, TYR407, ILE207, VAL303	-	PHE352, TYR69
16	**IND-15**	−8.678	25	ALA68, TYR69, MET350, PHE352, PHE208, ILE335, LEU337, CYS323, ILE325, LEU97, ILE180, TYR444, MET445,CYS406,TYR407, VAL303,VAL210, TRP397, ILE207	HOH726	PHE352, TYR69
17	**IND-16**	−8.612	25	ALA68, TYR69, PHE352, MET350,ILE180, VAL210, PHE208, LEU337, ILE335, LEU97, CYS323, ILE325, PHE108,ALA111,TYR444, MET445,CYS406,TYR407, VAL303	-	PHE352, TYR69
18	**IND-17**	−8.281	25	ALA68, TYR69, PHE352, MET350, ILE180, ILE335, LEU337, CYS323, ILE325, LEU97, VAL210, PHE208, TYR444,MET445,VAL303, TRP397, CYS406, TYR407	HOH726 PHE208 ARG51 THR336	PHE352,
19	**IND-18**	−8.265		ALA68, TYR69, PHE352, MET350, ILE180, LEU97, VAL210,PHE208, CYS323, ILE325, ALA111, TYR444, MET445,VAL303,CYS406, TYR407, ILE335, LEU337	HOH726 PHE252	PHE352,
20	**IND-19**	−8.195	25	ALA68, TYR69, PHE352, MET350, ILE180, ILE207, PHE208, ILE325, CYS323, VAL210, LEU337, ILE335, TYR444,MET445,TYR407, CYS406, VAL303	-	PHE352, PHE208, TYR69
21	**IND-20**	−8.054	26	ALA68, TYR69, PHE352, MET350, ILE335, LEU337, CYS323, ILE325, VAL210, PHE208, LEU97, ALA111, ILE180, TYR444, MET445, CYS406, TYR407, VAL303	-	PHE352, PHE208, TYR69
22	**IND-21**	−7.819	25	ALA68, TYR69, PHE352, MET350, ILE335, LEU337, CYS313, ILE325, ILE207, PHE208, VAL210, LEU97, ILE180, MET445, TYR444, CYS407, TYR407, VAL303	-	PHE352, PHE208, TYR69
23	**IND-22**	−7.816	24	ALA68, TYR69, PHE352, MET350, ILE335, LEU337, ILE325, CYS323, ALA111, VAL210, PHE208, ILE207, ILE180, TYR44, MET445, CYS406, TYR407, VAL303	-	PHE352, TYR69
24	**IND-23**	−7.789	26	ALA68, TYR69, PHE352, MET350, LEU337, ILE325, CYS323,VAL210, PHE208, ILE207, ILE180, VAL303, TYR444,MET445,CYS406, TYR407	HOH726 TYR69	PHE352, PHE208, TYR69
25	**IND-24**	−7.772	26	ALA68, TYR69, PHE352, MET350, LEU337, ILE335, ILE180, ALA111, VAL210, PHE208, LEU97, ILE325, CYS323,TYR444,MET445, TYR407, CYS406	-	PHE352, TYR69
26	**IND-25**	−7.519	26	ALA68, TYR69, PHE352, MET350, ILE325, CYS323, ALA111,PGE208,VAL210, LEU337, ILE335, TYR444, MET445,CYS406,TYR407, ILE180	PHE352	PHE352, TYR69

(contd.)

Table 5 — D-score of 30 ligands and type of interactions involved in MAO-receptor (*contd.*)

S.No	Compd	D-Score	No. Of Residues	Hydrophobic	Aromatic	Pi-Pi Stacking
27	**IND-26**	−7.477	24	ALA68, TYR69, PHE352, MET350, LEU337, ILE335, ILE180, ILE325, CYS323, VAL210, PHE208, LEU97, ALA111,TYR444,MET445, CYS406, TYR407, TRP397	HOH726	PHE352, PHE208, TYR69
28	**IND-27**	−7.366	25	ALA68, TYR69, PHE352, MET350, LEU97, PHE208, VAL210, CYS323, ILE325, LEU337, ALA111, ILE335, ILE180, TYR444, MET445, TYR407, CYS406	TYR69	PHE352, PHE208, TYR69
29	**IND-28**	−7.322	26	ALA68, TYR69, PHE352, MET350, ILE325, CYS323, ALA111, PGE208, VAL210, LEU337, ILE335, TYR444, MET445, CYS406, TYR407, ILE180	TYR69	PHE352, PHE208, TYR69
30	**IND-29**	−7.150	25	ALA68, TYR69, PHE352, MET350, LEU337, ILE335, PHE208, VAL210, LEU97, CYS323, ILE325, ALA111, ILE180, MET445, TYR444, CYS406, TYR407	TYR69	-
31	**IND-30**	−7.136	26	ALA68, TYR69, PHE352, MET350, LEU337, ILE335, CYS323, LEU97, ILE325, ALA111, VAL210, PHE208, ILE207, ILE180, MET445, TYR444, CYS406, TYR407, VAL303	-	PHE352, TYR69

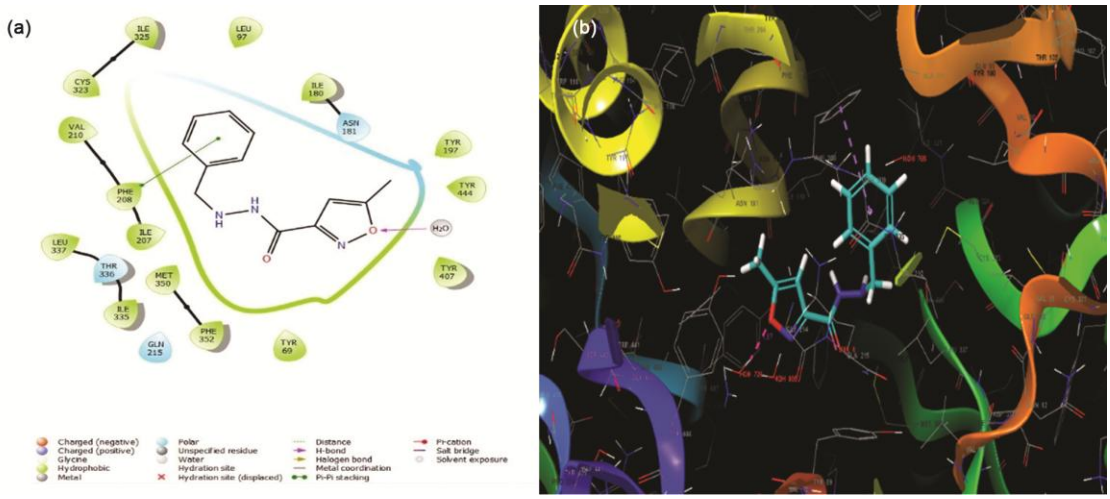

Fig. 4 — 2D (a) and 3D (b) representation of the interaction of Isocarboxazid with 2Z5X

of the drugs under clinical trials could not see the market due to failure at the stage of pharmacokinetic evaluation. Due to this impact on eventual success, these studies now occur early in the drug discovery process[23]. Initial screening of hits and leads before their clinical testing will not only decrease the rate of failure, but it reduces the cost of drugs discovery program[24]. The underlying goal and end-game for all ADME/Tox studies is to better understand a compound's metabolite-mediated toxicity and safety profile to make a concrete decision on whether the compound can progress to late stage preclinical and clinicalstudies to enable filing for an Investigational New Drug (IND), New Drug Application (NDA), or a Biologics Licensing Application (BLA)[25].

Taking into consideration, a preliminary predictive *in silico* pharmacokinetic study of the library generated compounds was undertaken using the Qik Prop module in Schrodinger software 12.3. Incorporation of such tools as a part of the drug design process can screen molecules that are more likely to exhibit satisfactory absorption, distribution, metabolism, excretion (ADME) properties[26]. The server calculated the parameters such as human oral absorption (HOA%), cellular permeability Caco-2 *in vitro*, cell permeability Maden Darby Canine Kidney (MDCK) *etc*. The results of ADME prediction

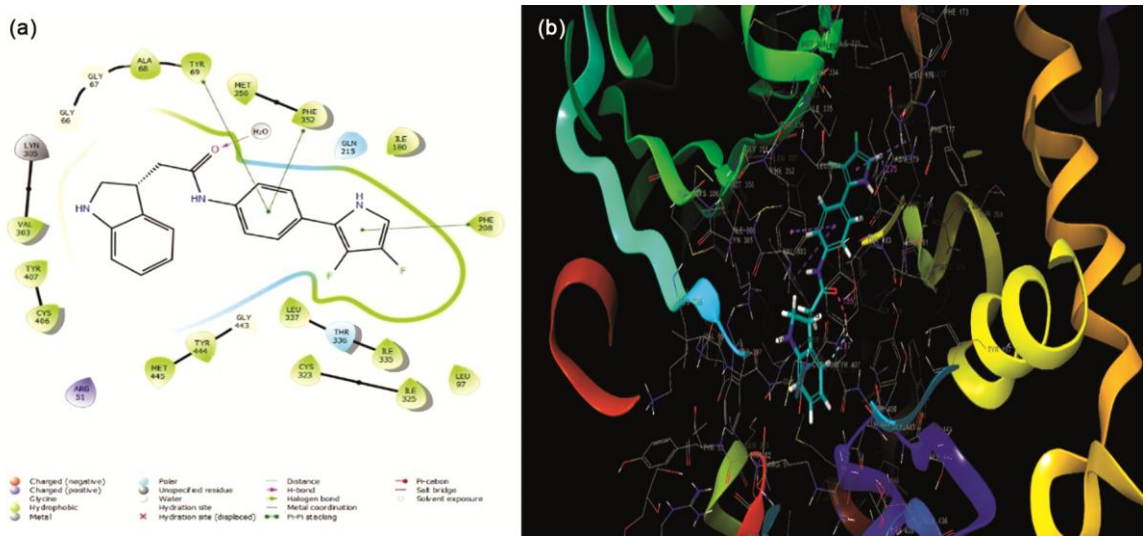

Fig. 5 — 2D (a) and 3D (b) representation of the interaction of ligand 1 with 2Z5

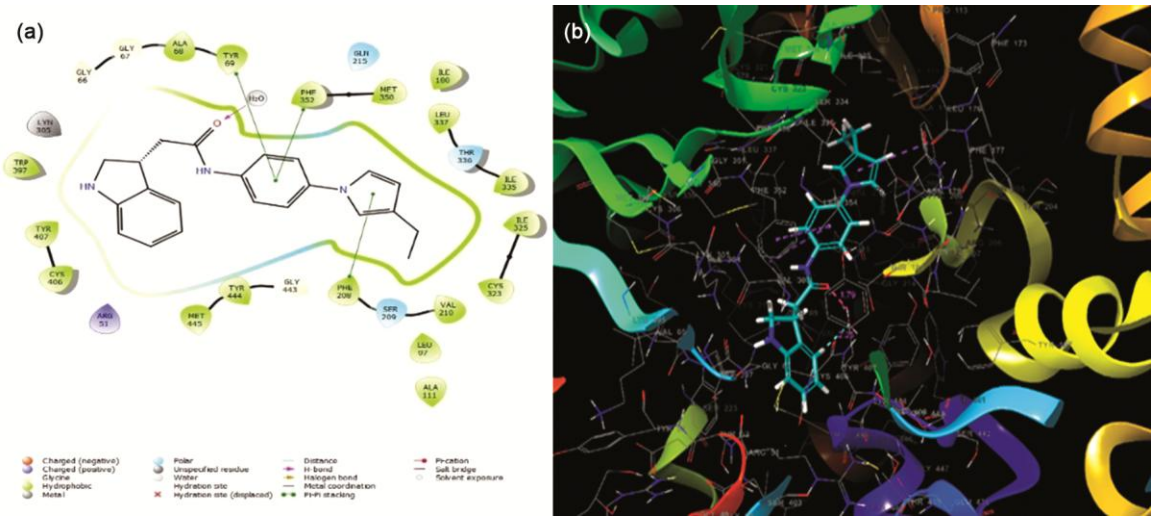

Fig. 6 — 2D (a) and 3D (b) representation of the interaction of ligand 2 with 2Z5X.

are shown in Table 6. The Schrodinger server calculated the properties, as a determinant for drug development factors like human oral absorption (HOA%), cellular permeability Caco-2 *in vitro*, cell permeability Maden Darby Canine Kidney (MDCK) *etc*. Mainly human intestinal absorption properties because it is determinant for the drug development that is purport to be administered orally[11]. The absorption process *i.e* permeation of compounds through biological membrane is influenced by the physicochemical characteristics, and present observation of HOA for all the compounds in the range of 95.54 to 100 indicate the good physicochemical properties of the compounds **(IND-1 to IND-30)** enabling them to qualified HOA% with values > 70-100%.

Caco-2 cells derived from human colon adenocarcinoma, have transport *via* intestinal epithelium and *in vitro* Caco-2 represents an important test to assess intestinal absorption of drugs. In general, good permeability was observed for the eleven hits with top D score as indicated in Table 6. However, **IND-23** with 603.224 with maximum Caco-2 values (<25 poor >500 great) may get maximum permeation through human colon adenocarcinoma.

QPPMDCK system with canine kidney cells having shorter growth than that of Caco-2 cells was used as a tool for the rapid analysis of permeability. Derivatives **IND-1, IND-4, IND-9, IND-10, IND-14, IND-22, IND-23, IND-24, IND-26, IND-28, IND-29**

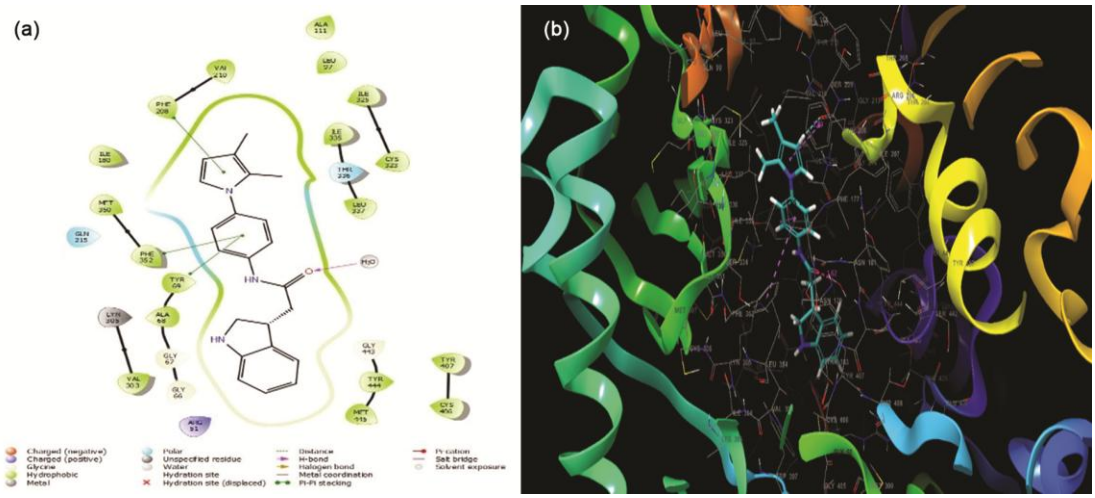

Fig.7 — 2D (a) and 3D (b) representation of the interaction of ligand 3 with 2Z5X

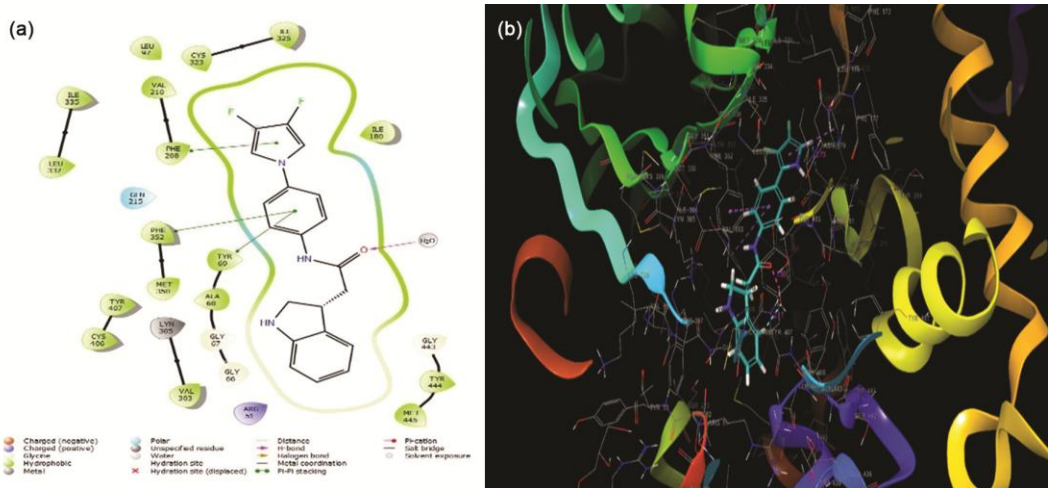

Fig. 8 — 2D (a) and 3D (b) representation of the interaction of ligand 4 with 2Z5X

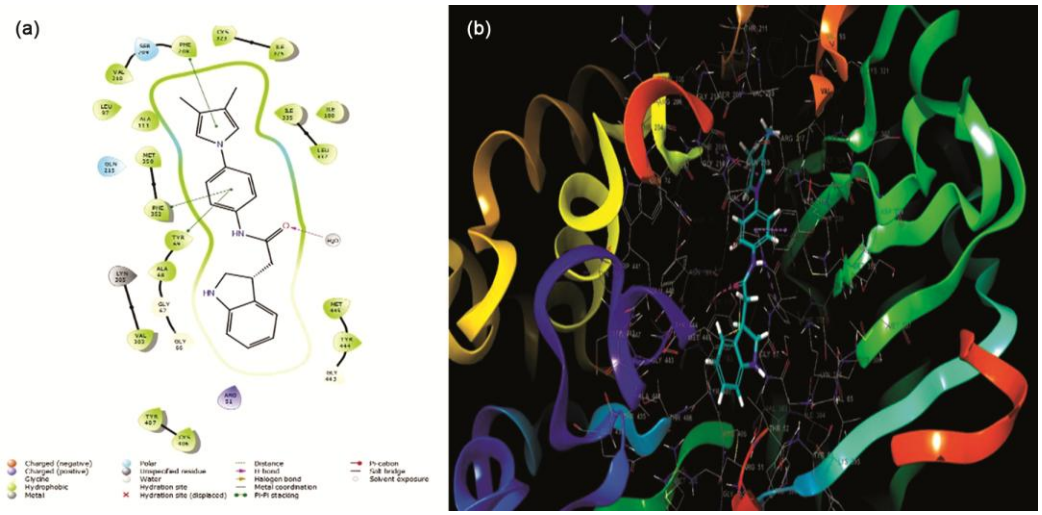

Fig. 9 — 2D (a) and 3D (b) representation of the interaction of ligand 5 with 2Z5X

Table 6 — ADME prediction of Isocarboxazid (reference) and 30 compounds

Compd	MOL MW	DHB	AHB	QPLOG PO/W	QPP CACO	QP LOGBB	QPP MDCK	% HOA	CNS	DIPOLE	VOLUME
Isocarboxazid (Reference)	231.254	2	5.0	2.511	394.320	−0.881	306.012	87.06	−1	2.100	825.431
IND-1	353.371	3	3.5	3.929	352.530	0.052	504.906	95.54	1	4.225	1103.410
IND-2	345.443	2	3.5	4.550	518.796	−0.054	269.262	100	1	7.081	1195.028
IND-3	345.434	2	3.5	4.384	514.885	0.027	267.069	100	1	7.157	1173.533
IND-4	353.371	2	3.5	4.390	512.753	0.261	897.377	100	1	9.025	1112.119
IND-5	350.46	2	4.2	4.340	546.161	−0.156	284.646	100	1	7.521	1223.187
IND-6	345.443	2	3.5	4.523	513.669	0	266.387	100	1	6.463	1196.385
IND-7	347.416	2	4.0	4.226	531.399	−0.096	276.339	100	1	5.227	1167.695
IND-8	348.401	2	4.7	3.671	522.376	−0.015	271.271	100	1	5.366	1131.408
IND-9	353.438	2	3.5	4.639	456.211	−0.056	375.116	100	1	7.317	1211.942
IND-10	342.440	2	3.5	4.438	597.991	0.012	313.952	100	1	3.123	1153.274
IND-11	345.443	3	3.5	4.163	402.472	−0.127	204.642	100	0	8.569	1190.750
IND-12	349.475	3	4.5	3.915	429.969	−0.311	219.796	100	0	6.065	1217.817
IND-13	346.428	2	4.0	3.858	519.687	0.080	269.761	100	1	5.95	1126.413
IND-14	353.438	3	4.5	3.855	493.462	−0.029	397.772	100	0	7.416	1178.879
IND-15	348.401	2	4.7	3.637	515.445	-0.008	267.382	96.784	1	5.372	1125.811
IND-16	345.443	2	4.0	4.288	573.904	−0.025	300.305	100	1	3.088	1177.631
IND-17	349.475	3	4.5	4.010	499.377	−0.181	258.385	100	0	5.765	1224.999
IND-18	349.475	2	3.5	4.411	475.995	0.004	245.333	100	1	6.07	1196.841
IND-19	350.460	2	4.2	4.318	515.434	−0.179	267.376	100	1	7.071	1223.194
IND-20	349.475	2	4.5	4.014	500.704	−0.092	259.127	100	1	5.990	1195.338
IND-21	349.475	2	4.5	4.170	510.748	−0.162	264.750	100	1	5.937	1218.818
IND-22	353.438	2	4.5	4.009	601.292	0.198	467.031	100	1	3.690	1166.652
IND-23	350.460	2	4.2	4.301	603.224	−0.074	316.923	100	1	4.857	1209.955
IND-24	345.443	2	4.0	4.048	594.758	0.137	312.118	100	1	6.436	1144.955
IND-25	345.443	3	3.5	4.002	407.923	−0.118	207.640	100	0	2.436	1156.346
IND-26	342.440	2	3.5	4.456	594.418	0.045	311.925	100	1	4.950	1164.759
IND-27	343.427	2	4.5	3.966	437.552	−0.130	223.988	100	1	6.816	1169.116
IND-28	347.391	2	4.5	3.912	439.535	0.003	407.174	100	1	5.296	1127.551
IND-29	350.460	2	5.2	3.586	589.759	0.021	309.283	100	1	5.71	1157.263
IND-30	350.460	2	4.2	4.201	521.136	−0.126	270.575	100	1	5.883	1204.594

may have higher permeability towards kidney cells as compared to reference drug 306.012 nm/sec, according to QPPMDCK permeability classification into low (<25 nm/sec) and mean (>25 to 500nm/sec)

Too polar drugs cannot cross the blood brain barrier (BBB) and prediction of blood/brain partition coefficients (log B/B) was important to access the central nervous system (CNS) permeability of these molecules. The computed and predicted CNS activity on an inactive (−2) to active (+2) scale showed that set of all the compounds **(IND-1 to IND30)** withpredicted CNS activity >1, could be active in the CNS. Further, parameters like molecular weights (MW), QPlogPo/w, lipophilicity (log P), number of hydrogen bond donors and acceptors were used to assess the "drug-likeness". Almost all the identified 30 compounds are satisfying the aforementioned qualifications and indicating drug able properties.

Molecular Simulation Studies

The docking studies based on 'lock and key' concept describes the interaction of small molecules with a stationary receptor without undergoing any conformational changes, but by overlooking the existence of any atomic movement. So, molecular dynamic simulations are carried out to analyse the physical movements of both the protein and ligand molecules and to observe the interactions for a fixed period of time is important for understanding the nature of their true interactions. After ligands binding, the dynamic behaviour of a protein was investigated by running the MD simulation, at 100 ns to confirm

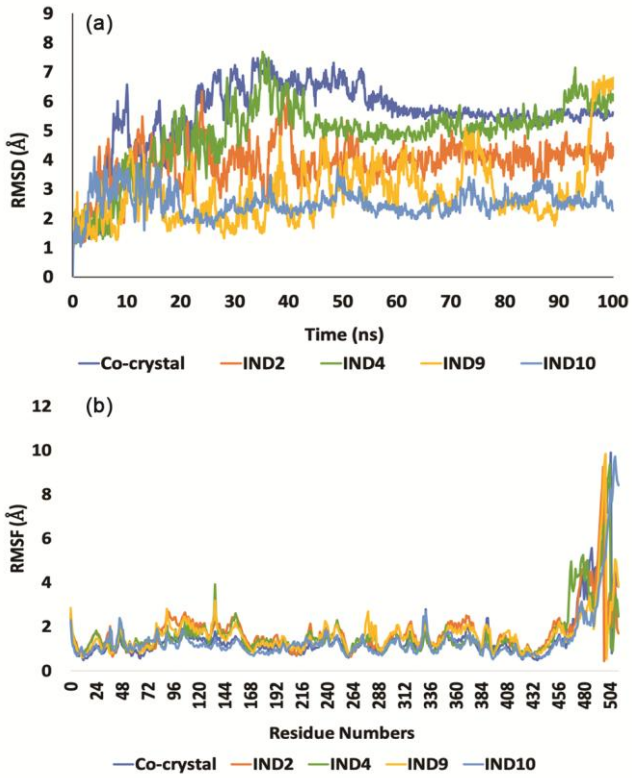

Fig. 10 — (a) RMSD and (b) RMSF plots of all the proteins in the protein-ligand complexes

the stability of the predicted binding of the ligand receptor complex system. The trajectories of the complexes were analysed on completion of the simulation in order to study the root mean square deviation (RMSD), root mean square fluctuation (RMSF), and protein-ligand interactions. The RMSD was determined for the backbone atoms of the protein co crystal IND2 IND4 IND 9 and IND 10 to evaluate their stability and conformational changes with respect to their docked ligands during MD simulation. The analysis of RMSD plot (Fig. 10) of the MD simulation indicated that complexes in all the simulations had stabilized at nearly 40 ns , except for IND 9 thus indicating the stable interaction with the protein.

All across the simulation, root means square fluctuation (RMSF) of the backbone atoms of the four complexes was also performed across the whole trajectory to assess the flexibility of the residues of these structures. RMSF analysis indicated that binding of designed protein-ligand complexes presented a somewhat non-significant fluctuation, which further reflects that there were no significant changes in protein conformation as a result of the ligand binding. A maximum fluctuation of 3.5 Å can be seen in Fig. 10(b) observed in the loop region of residue 130 and a high fluctuation was spotted in the terminal region close to residue 500 as expected. Though slight fluctuations were observed during the interaction of protein and designed compounds, but the majority of these fluctuations were lower than 3 Å, suggesting that strong binding exists between compounds and protein.

IND2 bound to the target protein using a combination of hydrogen hydrophobic and water bridged interactions. Fig. 11 is indicating the interaction of key residues like Tyr 69 and Tyr 407 through H-bond and water mediated interactions with TYR407 and GLY 443 of Chain A for 30% of the total simulation time. While Fig. 12 indicating the water mediated interactions between C=O (amide linkage) of **IND 4** with TYR69 of Chain A for 40% of the simulation time. Though two type of interactions *i.e* water mediated and H bond were observed with GLY 443, but mostly it was water bridged interactions with 58% fraction of total interactions. Additional water mediated interactions with GLN 215 (74%) of chain A were observed in **IND 9** (Fig. 13) along with interactions with key residue TYR 69 and GLY 443 in similar to that of **IND 4.** Despite more number of its interactions the protein–ligand IND9

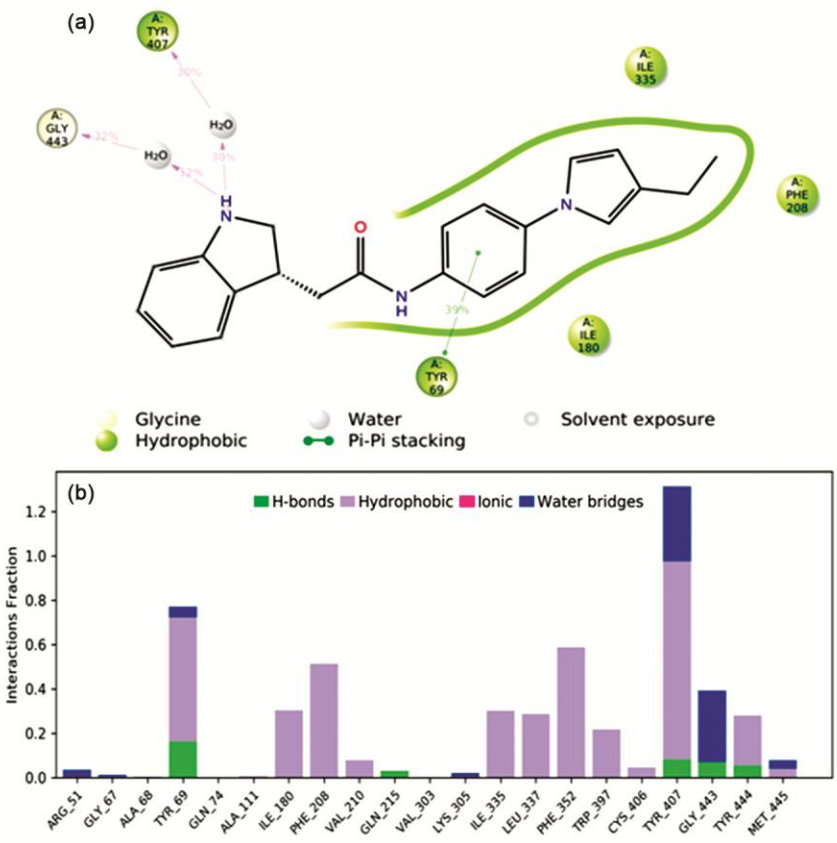

Fig. 11 — Protein ligand interactions of the compound IND2

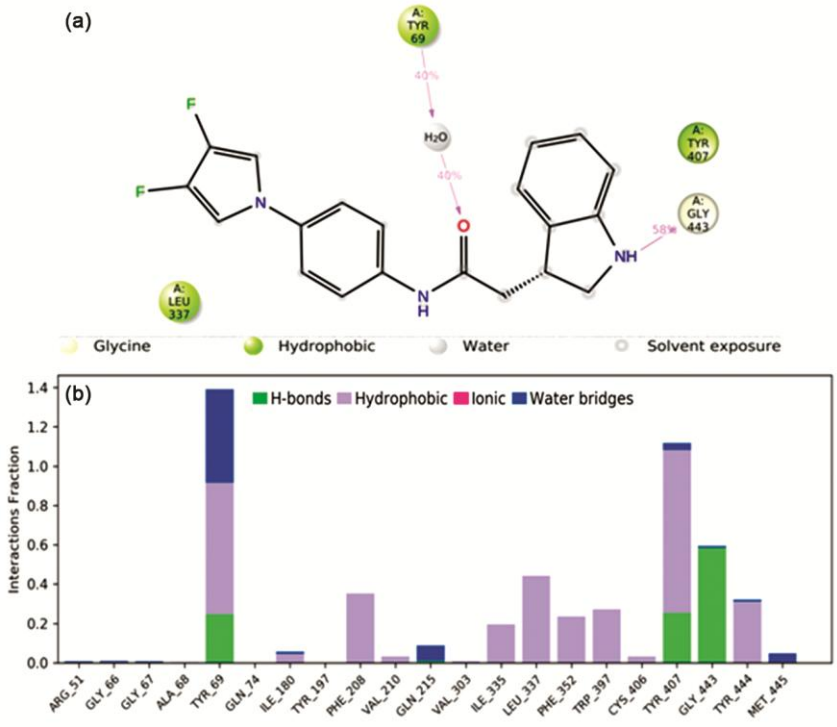

Fig. 12 — Protein ligand interactions of the compound IND4

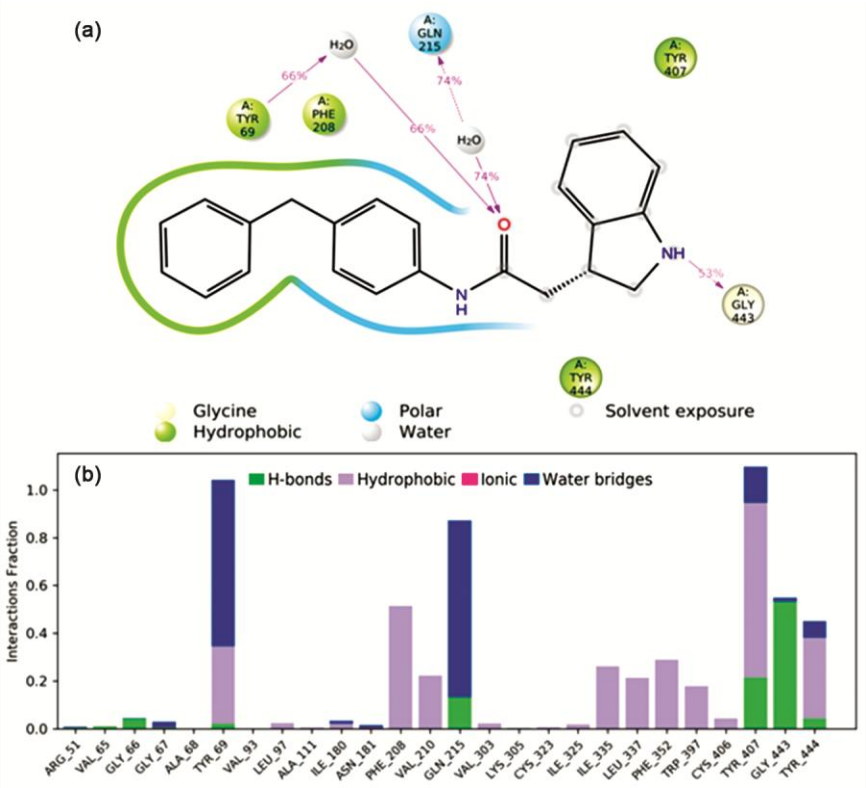

Fig. 13 — Protein ligand interactions of the compound IND9

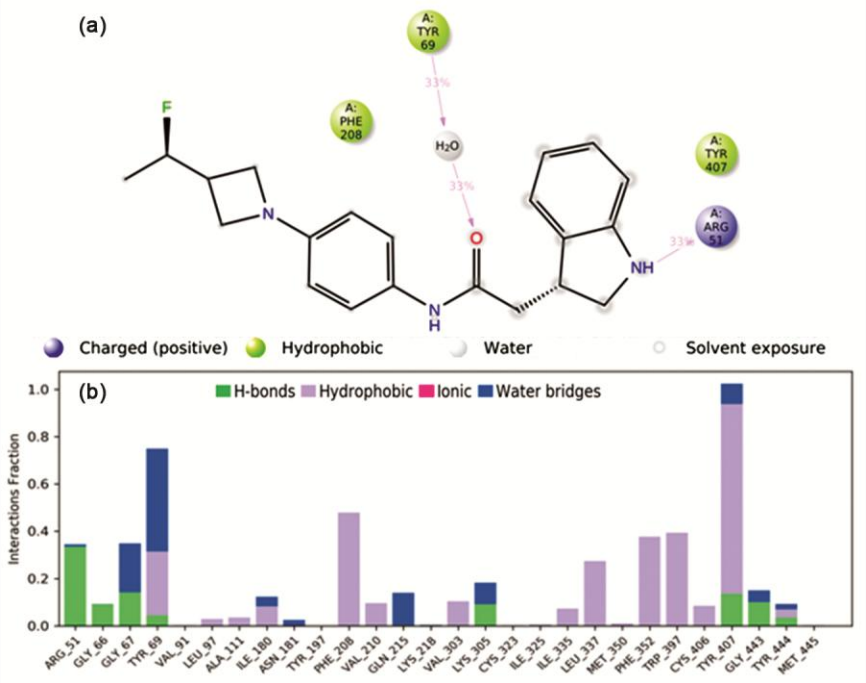

Fig. 14 — Protein ligand interactions of the compound IND10

complex not found to be stable (RMSD Plot Fig. 10)**.** **IND10-protien** complex was also found to be stable on account of H-bond type interactions with ARG 51 for 69% of the time, water mediated interaction with TYR 69 (33%) along with hydrophobic types with PHE 208 and TYR 407 as seen in Fig. 14.

Conclusions

The classical period of the MAO inhibitors began with hydrazine derivatives and resulted into the first antidepressant, Iproniazid. Nitrogen containing heterocyclic Indole scaffold with well documented wide spectrum biological activities have been found in most of the important synthetic drug molecules including antidepressant and paved a faithful way to develop effective targets, Thus, considering the importance of indole moiety and reported MAOIs activity of 4-(1H-benzimidazol-2-yl)-N-(substituted phenyl)-4-oxobutanamide derivatives with benzimidazole moiety, here in present study computational approaches were adopted to design and screen Indole-3-yl derivatives. The approaches were computationally efficient and allowed the screening of generated library of 1853 Indole derivatives using library enumeration module of the Schrodinger tool resources.

Library was screened and potent ligands were identified for MAO-A enzyme, that is considered a good model for treatment of depression. Based on computational docking and pharmacological profile prediction the top few **IND2, IND4, IND9, IND10, IND14, IND22, IND23, IND24, IND26, IND28** and **IND29** compounds were identified. MD simulation were performed on top four compounds with high D score and results showed their stable interaction with the key residues with acceptable range of RMSD, which was also supported by RMSF results.

The identified potent molecules would be synthesised, tested and validated over an experimentally *in vitro* and *in vivo* models. Detailed studies on these molecules can make a great impact in the field of medicinal chemistry for the development of MAO-A inhibitors and may provide us with new drug candidate for the treatment of depression

Contribution of authors

Alka Kumari performed the *in silico* studies and drafted the manuscript. Neelima Dhingra a corresponding author designed the concept and checked the manuscript. Priyanka Rana and Harnoor Kaur provided their technical support to run the software and helped me complete studies and proofreading the manuscript. Dr Tanzeer Kaur guided me in compiling the results and discussion. All authors have read and approved the manuscript.

Conflict of interest

The authors declare that they have no conflicts of interest with the contents of this article.

References

1 Richards D, *Clinical Psy Rev*, 7 (2011) 1117.
2 Bhowmik D, Sampath K P, Srivastava S, Paswan S & Dutta A S, *Depression : Symptoms, Causes, Medications and Therapies*, 1 (2012) 37-39.
3 Duarte P, Cuadrado A & León R, *Handbook Exp Pharm*, 264 (2020) 229. (https://doi.org/10.1007/164_2020_384)
4 Stahl S M & Felker A, *CNS. Spectr*, 13 (2008) 855.
5 Remick R A & Froese C, *Can Fam Phys*, 36 (1990) 1151.
6 Hubálek F, Pohl J, Edmondson D E, *J Biol Chem*, 278 (2003) 28612.
7 Sravanthi T V & Manju S L, *Eur J Pharm Sci*, 91 (2016) 1.
8 Kaushik N K, Kaushik N, Attri P, Kumar N, Kim C H, Verma A K & Choi E H, *Molecules.*, 18 (2013) 6620.
9 Nayak S, Shyama S K, Goyal P K, Vyas V & Chauhan C S, *Int J Pharm Erud*, 5 (2015) 25.
10 Mehta S & Pathak S R, *Asian J Pharm Clin Res*, 10 (2017) 335.
11 Chirkova Z V, Kabanova M V, Filimonov S I, Abramov I G, Petzer A, Petzer J P & Suponitsky K Y, *Bioorg Med Chem Lett*, 26 (2016) 2214.
12 Fan N, Zhang S, Sheng T, Zhao L, Liu Z, Liu J & Wang X, *Chem Biol Drug Des*, 91 (2018) 398.
13 Verma J, Khedkar V & Coutinho E, *Curr Top Med Chem*, 10 (2010) 95.
14 Zhao X, Chen M, Huang B, Ji H &Yuan M, *Int J Mol Sci*, 12 (2011) 7022.
15 Sippl W, *Recent Advances Media*, (2010) 103.
16 Chirkova Z V, Kabanova M V, Filimonov S I, Abramov I G, Petzer A, Engelbrecht I Petzer J P, Suponitsky K Y & Veselovsky A V, *Drug Dev Res*, 79 (2018) 81.
17 Kalirajan R, Sankar S, Jubie S & Gowramma B, *Indian J Pharm Educ Res*, 51 (2017) 110.
18 Ivanova L, Tammiku-Taul J, García-Sosa A T, Sidorova Y, Saarma M & Karelson M, *ACS Omega*, 3 (2018) 11407.
19 Thenmozhi M, *In Silico Investigation of Piperine Against Human Monoamine Oxidase-A (MAO-A) Enzyme – Vitiligo*, 2 (2014) 119.
20 Rathee D, Lather V & Dureja H, *Res Innov*, 1 (2017) 112.
21 Firdayani A A & Churiyah Y A, *J Young Pharm*, 10 (2018) 20.
22 Joshi T, Joshi T, Sharma P, Mathpal S, Pundir H, Bhatt V & Chandra S, *Eur Rev Med Pharm Sci*, 24 (2020) 4529.
23 Madhavi S G, Adzhigirey M, Day T, Annabhimoju R & Sherman W, *J Comp Aided Mol Des*, 27 (2013) 221.
24 Mitchell W, Zhao S X, Zelesky V, Whalen K M, West M, Umland J, Troutman M D, Taylor C,. Soglia J R, Steyn S J, Snyder M, Hop C E C A, Liston T E, Lebowitz R, Krueger S, Jenkins K, Janiszewski J S, Federico J, Duignan D B, Davidson R E & Cole M J, *Curr Drug Metab*, 9 (2008) 847.
25 Yeung A W K, Georgieva M G, Atanasov AG & Tzvetkov N T, *Front Mol Neurosci*, 12 (2019) 1.
26 Verma R, Bairy I, Tiwari M, Bhat G V & Gautha S G, *Mol Diversity*, 26 (2018) 1.